International Journal for Parasitology 44 (2014) 415–427

Contents lists available at ScienceDirect

International Journal for Parasitology

journal homepage: www.elsevier.com/locate/ijpara

Identification and pharmacological induction of autophagy in the larval stages of *Echinococcus granulosus*: an active catabolic process in calcareous corpuscles ☆

Julia A. Loos [a,b,1], Pedro A. Caparros [a,b,1], María Celeste Nicolao [a,b], Guillermo M. Denegri [a,b], Andrea C. Cumino [a,b,c,*]

[a] *Laboratorio de Zoonosis Parasitarias, Departamento de Biología, Facultad de Ciencias Exactas y Naturales, Universidad Nacional de Mar del Plata (UNMdP), Funes 3350, Nivel Cero, (7600) Mar del Plata, Argentina*
[b] *Consejo Nacional de Investigaciones Científicas y Técnicas (CONICET), Argentina*
[c] *Departamento de Química, Facultad de Ciencias Exactas y Naturales, Universidad Nacional de Mar del Plata (UNMdP), Funes 3350, Nivel 2, (7600) Mar del Plata, Argentina*

ARTICLE INFO

Article history:
Received 13 November 2013
Received in revised form 14 February 2014
Accepted 17 February 2014
Available online 1 April 2014

Keywords:
Echinococcus
Autophagy
Rapamycin
Arsenic trioxide
Calcareous corpuscles
Eg-Atg8 expression

ABSTRACT

Autophagy is a fundamental catabolic pathway conserved from yeast to mammals, but which remains unknown in parasite cestodes. In this work, the pharmacological induction of autophagy was cellularly and molecularly analysed in the larval stages of *Echinococcus granulosus*. Metacestode sensitivity to rapamycin and TORC1 expression in protoscoleces and metacestodes were shown. Ultrastructural studies showed that treated parasites had an isolation membrane, autophagosomes and autolysosomes, all of which evidenced the autophagic flux. Genes coding for key autophagy-related proteins were also identified in the *Echinococcus* genome. These genes were involved in autophagosome formation and transcriptional over-expression of Eg-*atg*5, Eg-*atg*6, Eg-*atg*8, Eg-*atg*12, Eg-*atg*16 and Eg-*atg*18 was shown in presence of rapamycin or arsenic trioxide. Thus, *Echinococcus* autophagy could be regulated by non-transcriptional inhibition through TOR and by transcription-dependent up-regulation via FoxO-like transcription factors and/or TFEB proteins. An increase in the punctate pattern and Eg-Atg8 polypeptide level in the tegument, parenchyma cells and excretory system of protoscoleces and in vesicularised parasites was detected after rapamycin treatment. This suggests the occurrence of basal autophagy in the larval stages and during vesicular development. In arsenic-treated protoscoleces, high Eg-Atg8 polypeptide levels within the free cytoplasmic matrix of calcareous corpuscles were observed, thus verifying the occurrence of autophagic events. These experiments also confirmed that the calcareous corpuscles are sites of arsenic trioxide accumulation. The detection of the autophagic machinery in this parasite represents a basic starting point to unravel the role of autophagy under both physiological and stress conditions which will allow identification of new strategies for drug discovery against neglected parasitic diseases caused by cestodes.

1. Introduction

Autophagy, an evolutionarily conserved lysosome-dependent recycling pathway, is a fundamental intracellular degradative process operating as a homeostatic mechanism in all eukaryotic cells. This process is involved in the turnover of cytoplasm and can eliminate denatured cytosolic proteins and entire damaged organelles (Xie and Klionsky, 2007). Autophagy serves as a cell survival mechanism in starved or stressed cells. Thus, a low level of constitutive or basal autophagy is important to provide nutrients during catabolism, produce ATP during starvation and generate signals for removal of apoptotic corpses. Autophagy also plays a role in development, differentiation, embryogenesis, determination of lifespan and even cell death. Due to its routine housekeeping function, autophagy is involved in preventing tissue degeneration, ageing and cancer (Meléndez and Levine, 2009).

☆ *Note:* Nucleotide sequence data reported in this paper are available in the GenBank database under GenBank Accession Numbers JF430439.1 (Eg-*atg*8.1), JF430440.1 (Eg-*atg*8.2) and JF430443.1 (Eg-*atg*12).

* Corresponding author at: Laboratorio de Zoonosis Parasitarias, Departamento de Biología, Facultad de Ciencias Exactas y Naturales, Universidad Nacional de Mar del Plata (UNMdP), Funes 3350, Nivel Cero, (7600) Mar del Plata, Argentina. Tel.: +54 223 4752426x450.
E-mail address: acumino@mdp.edu.ar (A.C. Cumino).

[1] These authors contributed equally to this work.

http://dx.doi.org/10.1016/j.ijpara.2014.02.007
0020-7519/

During autophagy initiation, a portion of the cytoplasm is surrounded by a flat membrane sheet, known as the isolation membrane (or phagophore in yeast). The isolation membrane is closed to form the emerging double-membrane vesicle called the autophagosome, which fuses with lysosomes to degrade its cytoplasmic contents. Eventually, the inner membrane of the autophagosome, together with the enclosed cargo, is degraded and the resulting macromolecules are released into the cytosol through lysosomal membrane permeases for recycling (Xie and Klionsky, 2007). The molecular machinery that enables the formation of an autophagosome in response to various autophagic stimuli is almost completely identified in yeast and is also being rapidly elucidated in higher eukaryotes, but at present, there is controversy about the organelle from which the membranes originate.

Many of the key signaling mechanisms for autophagy regulation in eukaryotic organisms appear to be conserved. These include both extra- and intracellular signals, such as the target of rapamycin (TOR) kinase protein, the class I and class III Phosphatidylinositol 3-kinase (PI3K), the insulin-like growth factor-I receptor (IGF-IR), Ras and AMP-activated protein kinase (AMPK) (He and Klionsky, 2009; Yang and Klionsky, 2010). The TOR and class I PI3K pathways (through protein kinase B/Akt) negatively regulate autophagy when nutrients and growth factors are in high concentrations. In addition, TOR integrates inputs from many nutrients and growth factors via the class I PtdIns3K signaling and amino acid-dependent signal pathways. TOR exerts its function by forming two functionally and structurally different complexes highly conserved from yeast to mammals (Betz and Hall, 2013). Each complex phosphorylates a different set of substrates to regulate cell growth and metabolism in response to environmental cues. TOR complex 1 (TORC1), regulates cellular processes related to growth (activated by growth factors and amino acids) and stress response pathways, and TORC2, which has a role in insulin signaling, regulates cell proliferation and survival by phosphorylating the kinase Akt/PKB (Sarbassov et al., 2006). Thus, high TORC1 signaling equates to rapid growth, whereas reduced TORC1 activity instead enhances the proteasome-mediated turnover and autophagy. The small GTPase Ras has opposing functions in autophagy regulation: it inhibits autophagy by activating the PtdIns3K–PKB/Akt–TORC1 pathway, whereas it may induce autophagy via the Raf-1–MEK1/2 [mitogen-activated protein kinase/ERK (extracellular-signal-regulated kinase) kinase 1/2]–ERK1/2 pathway. The tyrosine kinase IGF-IR, upon association with insulin/IGF, undergoes autophosphorylation and becomes activated, leading to the stimulation of Ras and class I PtdIns3K, consequently inhibiting the autophagic process. Furthermore, the insulin/IGF-1 pathway blocks the activity of its downstream transcription factors, the Forkhead box transcription factor class O (FoxO), which are direct positive modulators of the transcription of some autophagic genes. Another sensor of cellular energy status is AMPK. It activates autophagy through direct and indirect inhibition of TORC1, positively modulating Atg1/Ulk1. On the other hand, MEK1/2 and class III PI3K, together with the protein Atg6/Beclin1, positively regulate autophagy and play a crucial role in the early steps of autophagosome formation (Meléndez and Levine, 2009). The autophagic proteins involved in autophagosome formation consist of several functional units: Atg1/Ulk1 kinase and its regulators (which induce autophagy), the PI3K-III complex (involved in vesicle nucleation), the Atg9 and Atg2-Atg18 complex (required in membrane cycling), and two ubiquitin-like conjugation systems, Atg12 and Atg8/LC3 (needed for vesicle expansion and vesicle completion) (Mizushima et al., 2011).

Under nutrient-rich conditions, Atg8 (whose mammalian orthologs are Microtubule-Associated Protein 1-Light Chain 3 (MAP1-LC3), Gamma-AminoButyric-acid-type-A-Receptor-Associated Protein (GABARAP) and Golgi-Associated aTpase Enhancer of 16 kDa (GATE16) is delivered into the cytosol. Upon autophagy induction, Atg8 largely exists as the membrane-associated form (conjugated with phosphatidylethanolamine – Atg8–PE) and is localised on both sides of the isolation membrane. Atg8 controls the size of the autophagosome and its lipidation is widely used to monitor autophagy induction (Nakatogawa et al., 2007). Additionally, under starvation and stress conditions, the autophagy-related genes are rapidly up-regulated at a transcriptional level; FoxO being the first transcription factor that is necessary and sufficient to induce autophagy in the larvae of *Drosophila melanogaster* and *Caenorhabditis elegans* (Klionsky et al., 2012).

Autophagy has previously been identified and described in detail in invertebrate model organisms (Al-Adhami et al., 2005; Zhang et al., 2009; Malagoli et al., 2010). In *C. elegans*, autophagy occurs at basal levels in most tissues during normal growth conditions, but is rapidly up-regulated in response to certain types of environmental stress (Kovacs and Zhang, 2010). Gene knockdown studies on this biological model have been crucial to verify the functions of autophagy in this multicellular organism. *Caenorhabditis elegans* has a single ortholog of most yeast Atg proteins, but two homologs of *atg*-4, *atg*-8 and *atg*-16 (Meléndez and Levine, 2009).

In cestodes, transmission (TEM) and scanning electron microscopy (SEM) data supported the theory that autophagy appears in the intracellular formation of calcareous corpuscles (McCullough and Fairweather, 1987), biomineralised parenchyma cells with specialised functions in larval physiology. This theory has also been accepted by the research group led by Sylvia Richards (Richards et al., 1984; Rogan and Richards, 1986; Smith and Richards, 1993) in ultrastructural studies of the parasite *Echinococcus granulosus*, the causative agent of cystic echinococcosis.

Cystic echinococcosis or hydatidosis is a widely endemic infection caused by the larval stage of *E. granulosus*, which produces clinical disease in humans and economic losses to the livestock industry. In search of therapeutic solutions for this disease, our research group has determined that rapamycin (Rm) is an effective scolicidal agent against *E. granulosus*, and that rapalogs increase the accumulation of cytoplasmic acidic organelles in a dose-dependent manner, suggesting that Rm induces autophagy in the parasite (Cumino et al., 2010). In mammalian cells, Rm forms an intracellular complex with the peptidyl-prolyl isomerase FKBP12 which binds to the FRB domain of mTOR (Choi et al., 1996). This induces a conformational change in mTOR complex 1 (mTORC1), which alters the interaction with its scaffolding protein, the regulatory associated protein of mTOR, and Lethal with Sec Thirteen protein 8 (raptor and LST8, respectively) (Hara et al., 2002). Thus, Rm exposure destabilises mTORC1, inducing autophagy (Nyfeler et al., 2011). In this study, we describe pharmacologically induced autophagy in the larval stages of *E. granulosus*. We also show the anti-echinococcal effect of Rm in metacestodes and verify the autophagic activity in calcareous corpuscles of this human parasite.

2. Materials and methods

2.1. In vitro culture of protoscoleces, metacestodes and pre-microcyst obtainment

Echinococcus granulosus protoscoleces were removed under aseptic conditions from hydatid cysts of infected cattle presented for routine slaughter at the abattoir in the province of Buenos Aires, Argentina. Protoscolex in vitro culture (n = 3,000/9.5-cm^2 growth area per well), pharmacological treatment and vitality assays were performed as previously described (Cumino et al., 2010). In vitro protoscolex treatments were assayed with 1, 5 and 20 μM Rm for 6, 4 and 2 days and with 0.05, 0.5 and 3 μM arsenic trioxide (As_2O_3) for 24, 12 and 3 h, respectively. Otherwise, *E.*

granulosus metacestodes (10–20 cysts for each drug treatment) obtained from the peritoneal cavities of CF-1 mice after i.p. infection with protoscoleces (Nicolao et al., 2014), were in vitro treated with 1, 5, 10 and 20 μM Rm. Animal procedures and management protocols were carried out in accordance with National Health Service and Food Quality (SENASA) guidelines, Argentina. Viability was assessed daily through an inverted light microscope on the basis of germinal membrane integrity for 7 days (until the viability control was lower than 90%). SEM and TEM were carried out with samples taken after 12 h of incubation (Cumino et al., 2010). For molecular experiments, parasites were washed with sterile and RNAse-free PBS and conserved at −80 °C until experimental use. For controls in all cases, parallel cultures of protoscoleces and metacestodes were treated with an equivalent volume of vehicle. Each experiment was performed using three replicates per treatment condition and repeated three times.

Incubation of protoscoleces with insulin and FBS for several days induces a progressive differentiation towards the metacestode stage or microcyst. Microcysts represent the phase in which the protoscolex is completely transformed into a miniature cyst (loosing suckers, rostellum and hooks, and showing a laminated layer), but the success rate of protoscoleces undergoing this dedifferentiation process is very low (1–3%). However, a previous differentiation stage, named pre-microcysts, can be obtained more easily. A pre-microcyst, a vesicle-like structure, is a completely vesicularised protoscolex with suckers and rostellum vestiges, without a laminated layer and almost devoid of movement. In order to obtain vesicularised protoscoleces and pre-microcysts, protoscoleces (n = 1,500/25-cm^2 growth area per bottle) were cultured in medium 199 supplemented with antibiotics (penicillin, streptomycin and gentamicin; 100 μg/ml), glucose (4 mg/ml), insulin (1.2 U ml^{-1}) and 15% FBS. Cultures were maintained at 37 °C for 50 days and the medium was changed every 5–7 days. Meanwhile, the number of developed pre-microcysts was determined by observation under an inverted light microscope at different time points. After 35–40 days, pre-microcysts developed under in vitro conditions were recovered and used for immunohistochemistry studies.

2.2. Gene identification, cloning and expression by reverse transcription (RT)–PCR and quantitative (q)PCR

The *Echinococcus multilocularis* genomic database, *E. granulosus* assembled genomic contigs (http://www.sanger.ac.uk/Projects/Echinococcus) and available sequences in the Expressed Sequence Tag (EST) database of *E. granulosus* (http://www.nematodes.org/NeglectedGenomes/Lopho.php) were searched with BLASTp and tBLASTn programs in order to obtain information on expressed *Echinococcus raptor*, *tor*, *fkbp*, *foxO* and *atg*1 to *atg*18 sequences. Sequences of *Homo sapiens*, *Bombyx mori*, *D. melanogaster*, *Schistosoma japonicum* and *Saccharomyces cerevisiae* were used as queries. We identified a single sequence for each putative gene, including *atg*1 to *atg*9, *atg*12, *atg*16, *atg*18, *raptor*, *tor*, *fkbp* and *foxO*, but two homologs of *atg*8. Specific primers were designed and are listed in Supplementary Table S1.

Total RNA extractions, RT–PCR, cloning and qPCR were performed as previously described (Cumino et al., 2010). To analyse the levels of gene expression in control and As_2O_3- and Rm-treated parasites, cDNA was generated from 10 μg of total RNA using Superscript II reverse transcriptase (Invitrogen, Argentina) and Pfu (Promega, USA) DNA polymerase. Equal amounts of cDNA from protoscoleces and metacestodes were amplified in 30 cycle PCRs of 94 °C (30 s), 45 °C (1 min), and 72 °C (1 min) plus a single step at 72 °C for 10 min. *Echinococcus granulosus* actin I (*actI*, GenBank Accession No. L07773) was used as a loading control. RT–PCR products were electrophoresed, purified using a Qiaquick PCR Purification Kit (Qiagen No. 28104, Argentina) and sequenced (Unidad Genómica INTA – Castelar, Argentina). In addition, qPCR experiments from protoscoleces were carried out in a StepOne Applied Biosystems cycler. The second reaction mixture contained 2 μl of cDNA, 12.5 μl of real mix (containing 0.1 μl of Taq DNA polymerase, Taq DNA polymerase buffer, 3 mM $MgCl_2$, 0.2 mM dNTPs and SYBR® Green™) and 50 pmol of each primer for each gene. The PCR programme was at 95 °C (10 min), 40 cycles at 95 °C for 15 s, 50 °C for 30 s, and 72 °C for 30 s. Product identification was confirmed by a melting curve analysis and visualised on agarose gels. The relative rate of each cDNA was normalised using *actI* (see above). Data analyses for a relative quantification of gene expression were performed by the comparative threshold cycle (Ct) method.

2.3. Sequence analysis

Ortholog selection was based on reciprocal best BLAST hits and the presence of the characteristic domains in each deduced amino acid sequence. A list containing all of the identified *E. granulosus* genes analysed both manually and by BLASTp (after joining the conceptual translation of exons) against the GenBank nr (non-redundant) database is shown in Supplementary Table S2. Sequence alignments were generated with the CLUSTALX software program. Modelling of tertiary structures was obtained from the deduced primary structure using the Gen-THREADER (SWISS-PROT). Analyses of prediction of transmembrane regions were realised with the TMHMM Server v. 2.0 (http://www.cbs.dtu.dk/services/TMHMM) and the SACS HMMTOP program (http://www.sacs.ucsf.edu/cgi-bin/hmmtop.py). Nuclear localisation signal (NLS) was predicted with cNLS Mapper Prediction (http://nls-mapper.iab.keio.ac.jp/cgi-bin/NLS_Mapper_form.cgi).

2.4. Western blot analysis and immunohistochemistry

Polypeptides were separated by SDS–PAGE on 15% polyacrylamide gels and electroblotted onto a nitrocellulose membrane (Hy-Bond C; Amersham, Argentina) as previously described (Cumino et al., 2010). The membranes were incubated with primary polyclonal antibody directed against the N-terminus of human LC3 (MAP LC3β antibody H-50, Santa Cruz sc-28266, USA, 1:1,000 dilution) or with primary monoclonal antibody of human actin (JLA-20, Developmental Studies Hybridoma Bank-DSHB, USA, 1:2,000 dilution) as a control for protein loading. The anti-LC3β antibody used in these assays is directed against an epitope which showed 52% amino acid identity with the N-terminus of the possible orthologs of *E. granulosus*. Additionally, control and Rm-treated protoscoleces were histologically processed as described in Nicolao et al. (2014). The deparaffinised-rehydrated sections were incubated overnight at 4 °C with the primary antibody anti-LC3 (1:500 dilution) and revealed with a secondary anti-rabbit IgG antibody conjugated with alkaline phosphatase (Bio-Rad 170-6518, USA, 1:500 dilution). In parallel, for in toto immunohistochemistry, protoscoleces were fixed in 4% (w/v) paraformaldehyde in 0.1 M PBS (pH 7.4) for 4 h at 4 °C, and then washed for 24 h at 4 °C in permeabilising solution (PBS at pH 7.4 containing 0.3% v/v Triton X-100, 0.2% w/v sodium azide and 0.5% w/v BSA). Control and pharmacologically treated protoscoleces were incubated for 3–5 days at 4 °C with the same primary antibody (1:50 dilution), and washed with PBS for 24 h at 4 °C. Finally, protoscoleces were incubated with goat anti-rabbit IgG conjugated with Alexa 488 for 24 h at 4 °C, washed and counterstained with 2 μg ml^{-1} propidium iodide (Molecular Probes P-3566, Argentina, to observe all cell nuclei under optimal contrast conditions). They were observed with an inverted confocal laser scanning microscope (Nikon, Confocal Microscope C1). Negative

controls consisted of omission of primary antibody for both experiments.

2.5. SEM and energy dispersive X-ray (EDX) analysis

For calcareous corpuscle microanalysis, protoscolex samples were processed according to the method of Smith and Richards (1993) with some modifications. Control and pharmacologically treated protoscoleces were fixed for 24 h with Karnovsky's solution, washed with buffer cacodylate 0.1 M, dehydrated and embedded in Histoplast® Plus at 60 °C. Thick sections (5 μm) were obtained, mounted, deparaffinised and coated with gold. Control and As_2O_3-treated specimens were viewed and analysed in the SEM mode of a JEOL JSM-6460LV electron microscope adapted with X-ray Energy Dispersive Spectroscopy (EDS) operating at 40 kV. The system used was an EDX Genesis XM4-Sys 60, equipped with Multichannel Analyzer EDX mode EDAM IV, Sapphire Si (Li) detector and Super Ultra Thin Window of Be, and EDX Genesis version 5.11 software.

2.6. Statistics

Data within experiments were compared; significance was determined using the t test and $P < 0.05$ was considered statistically significant. All data are shown as the arithmetic mean ± S.E.M.

3. Results

3.1. Pharmacological sensitivity to Rm in metacestode viability and TORC1 expression

The anti-echinococcal activity of Rm was tested in *E. granulosus* metacestodes maintained in vitro and observed over 1 week. Metacestode viability decreased as a function of Rm concentration (Fig. 1Ab), with 1 μM being the lowest concentration at which viability was reduced after 5 days incubation. At 10 μM, Rm had a pharmacological effect after 24 h (Fig. 1Aa). At a twofold higher concentration (20 μM), metacestodes presented detachment of the germinal layer in 90% of the cysts (Fig. 1B). Untreated metacestodes remained at least 90% viable throughout the experiment. Studies by SEM revealed that control metacestodes exhibit no ultrastructural alterations in parasite tissue during the whole incubation period (Fig. 1Ca,b). On the contrary, the germinal layer of treated metacestodes lost the multicellular structure feature (Fig. 1Cc,d).

Rm susceptibility is useful to dissect the cellular role of Eg-FKBP and possible TORC1 in *E. granulosus*. In order to determine metacestode Eg-*fkb1* expression as well as Eg-*tor* and Eg-*raptor* expression in both larval stages, RT–PCR assays were carried out. These genes were expressed in both protoscoleces and metacestodes (Fig. 1D).

3.2. Autophagic structures in Rm-treated protoscoleces and metacestodes

The tegument ultrastructure and its associated glycocalyx in control protoscoleces appeared unaltered. Fig. 2A and B show TEMs of untreated protoscoleces with microtriches projecting from their tegument and with glycogen deposits in the tegumental cells. Major effects of Rm include the appearance of several lysosomes and an expanded endoplasmic reticulum with developing autophagosomes (Fig. 2C). Lysosomes were recognisable by their high electron density, as well as their ovoid to pleomorphic or irregular shape. The distal cytoplasm of some cells was severely affected by the drug, showing loss and contraction of its integrity (Fig. 2D). Electron micrographs of developing autophagosomes surrounded by rough endoplasmic reticulum and autophagosomes containing cytoplasmic content are shown in Fig. 2E and F, respectively. Fig. 2E shows early or initial autophagic compartments such as the isolation membrane, a flat membrane cistern wrapping around a portion of cytoplasm. Fig. 2F illustrates the presence of an autophagosome, a late or degradative autophagic compartment limited by a double-membrane which contains partially degraded cytoplasmic material.

The germinal membranes of control metacestodes maintained their normal ultrastructural characteristics such as truncated microtriches intimately joined to the laminate layer, distal cytoplasm delimited by a basal membrane, muscle cells parallel to the cyst surface and numerous glycogen particles in the tegumental cells (Fig. 3A). However Rm-treated metacestodes presented disorganised muscle fibres, nuclei disappearance and tegumentary cell atrophy (Fig. 3B), as well as autophagic features such as intracellular vacuolisation and double-membrane structures containing electron-dense material (residual bodies, Fig. 3C) or lamellar stacks (similar to a tubular array of lamellar structures, Fig. 3D), indicating an advanced stage of degeneration compared with controls.

3.3. Occurrence and expression of key genes involved in Echinococcus autophagy and possible transcriptional regulation by Eg-FoxO

Since Rm is an allosteric inhibitor of TORC1, it is conventionally used as a positive control to induce autophagy. Thus, we analysed the occurrence of this process under control and pharmacological conditions in *Echinococcus* larval stages.

Extensive BLASTp searches on the available *E. multilocularis* genome and the incompletely assembled *E. granulosus* genome revealed the fundamental genes coding for autophagic proteins (Eg-Ulk2, Eg-Tor, Eg-raptor, Eg-Lst8, Eg-Atg6, Eg-Vps34, Eg-Vps15, Eg-Atg3, Eg-Atg4, Eg-Atg7, Eg-Atg8.1 Eg-Atg8.2, Eg-Atg5, Eg-Atg12, Eg-Atg16, Eg-Atg9, Eg-Atg2, Eg-Atg18; Supplementary Table S2). These genes were clustered in the different autophagosome formation steps: induction, vesicle nucleation, autophagosome expansion and membrane recycling. Ortholog selection was based on reciprocal best hits in BLAST searches, using an *E*-value cutoff $\leqslant 1e^{-25}$. We failed to find close relatives of yeast *atg*11, *atg*29, and *atg*31 and the human *atg*101, *atg*17/FIP200, *atg*10 and *atg*13. Three ESTs were obtained from *E. granulosus Lopho DB*, Eg-*atg8*.1, Eg-*atg8*.2 and Eg-*atg*12 (EGPSgr-4h05.p1k, EGCWgr-10c09.p1k and EGPSPgr-4a02.p1k, respectively), and also identified in the *E. granulosus* genome (pathogen_EgG_scaffold_0007 at 3941985–3942665, pathogen_EgG_scaffold_0029 at 270854–275012, and pathogen_EgG_scaffold_0005 at 6472092–6472427, respectively). These coding regions were cloned, fully sequenced and annotated in GenBank (JF430439.1, JF430440.1 and JF430443.1). Therefore, we identified two homologs to Atg8/LC3 encoding genes from the *E. granulosus* genome, annotated as EgrG_000551400 and EgrG_001158000 in the GeneDB database, with their respective orthologs in *E. multilocularis* (EmuJ_000551400 and EmuJ_001158000, see Supplementary Table S2). These two genes encode a 116 amino acid protein (named Eg-Atg8.1 and annotated as AER10558 in this work) and a 205 amino acid predicted protein (annotated as EgrG_001158000 in GeneDB database), respectively. However, we identified a coding sequence from protoscoleces (named Eg-*atg*8.2 and annotated as JF430440.1) with 118 amino acid, also included in EgG_scaffold_0029, but with a different nucleotide sequence in the C-terminal end. Thereby the 205 amino acid predicted protein could have gene prediction errors in accordance with the sequencing data of this work (data not shown). Subsequent studies will be carried out to analyse the possible alternative splicing and Eg-*atg*8.2 gene expression.

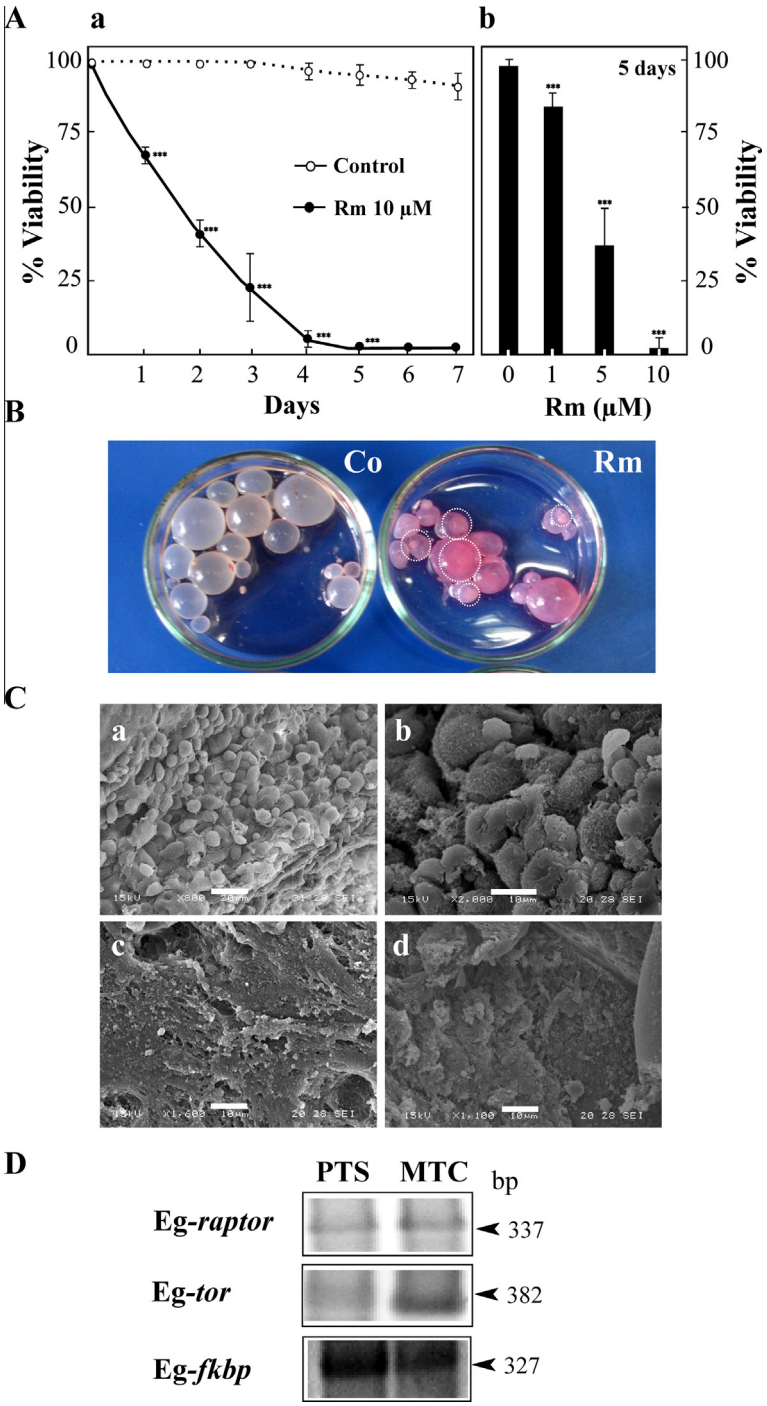

Fig. 1. Metacestode sensitivity to rapamycin (Rm) and TORC1 expression in *Echinococcus granulosus* larval stages. (A) Viability of metacestodes (measured on the basis of germinal layer integrity) incubated with 10 µM of Rm for 7 days (a) and 1, 5 and 10 µM Rm by the fifth day (b). Data are the mean ± S.D. of three independent experiments. ***Statistically significant difference ($P < 0.05$) compared with control. (B) Macroscopical damage of Rm-treated metacestodes during 24 h. Control metacestodes (Co) without morphological changes and metacestodes treated with 20 µM Rm showing increased permeability and collapsed germinal layer (circles). (C) Representative images of control (a and b) and Rm-treated metacestodes (c and d) obtained by scanning electron microscopy after 12 h of incubation. Ultrastructural damage appeared earlier than germinal layer detachment in metacestodes treated with 20 µM Rm. Bars indicate: 20 µm in (a) and 10 µm in (b–d). (D) Reverse transcription–PCR analysis from total RNA of control protoscoleces (PTS) and metacestodes (MTC). Eg-*fkbp*, Eg-*raptor* and Eg-*tor* gene expression was confirmed after 3 days of incubation in both larval stages.

RT–PCR analysis indicated expression of all identified Eg-*atg* genes in protoscoleces and metacestodes (Fig. 4A). qPCR showed higher mRNA expression levels for Eg-*atg*5 (threefold), Eg-*atg*6 (threefold), Eg-*atg*8.1 (fivefold), Eg-*atg*12 (sixfold) and Eg-*atg*16 (threefold) in 20 µM Rm-treated protoscoleces than in controls (Fig. 4B). Moreover, autophagy was induced by treatment with 1 and 5 µM Rm after 6 and 4 days, respectively. We found that the transcript levels for Eg-*atg*6, Eg-*atg*8.1 and Eg-*atg*12 increased one, two and twofold with 1 µM Rm and two, three and fourfold with 5 µM, respectively (Fig. 4C). No changes were detected for Eg-*atg*1, Eg-*atg*2, Eg-*atg*3, Eg-*atg*4, Eg-*atg*7, Eg-*atg*9 and Eg-*atg*18 between control and Rm-treated protoscoleces (data not shown). Similar expression patterns for the Eg-*atg* studied genes were observed in metacestodes (Fig. 4A).

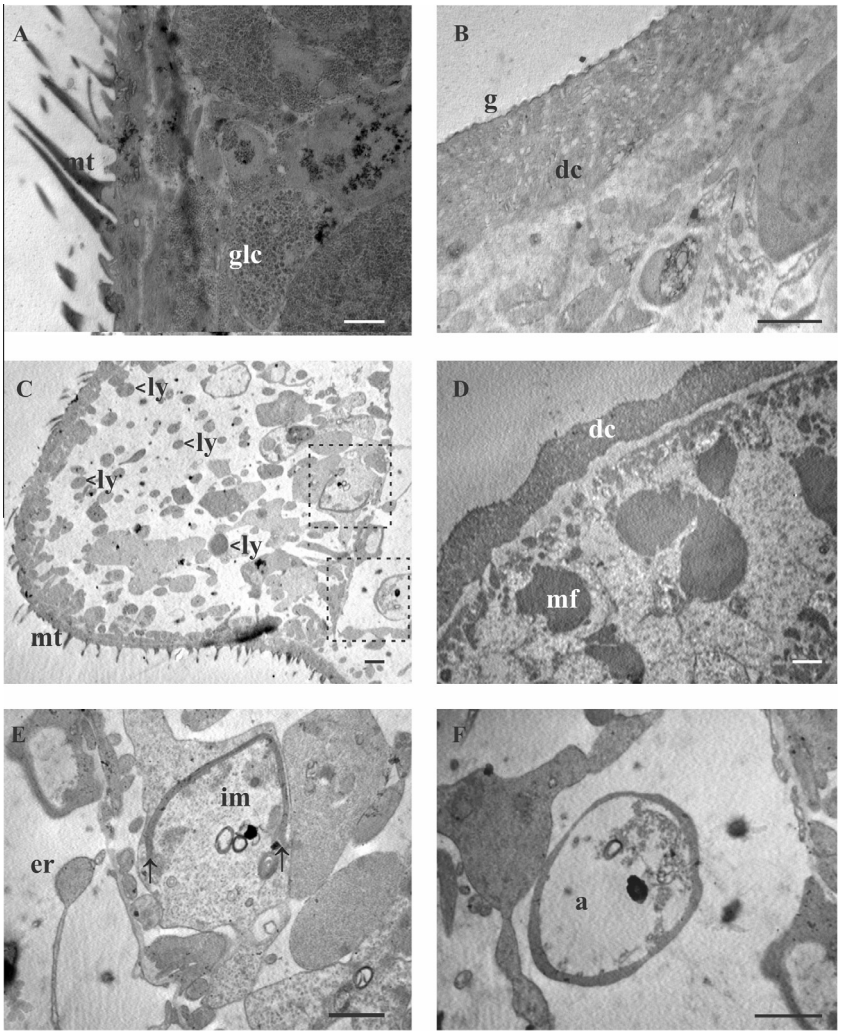

Fig. 2. Ultrastructural identification of autophagic structures in rapamycin (Rm)-treated *Echinococcus granulosus* protoscoleces. Transmission electron microscopy of control protoscoleces and treated with 20 μM Rm for 12 h. (A) Scolex region and (B) the soma from control protoscoleces exhibiting intact parasite tissue. In C–F, the damage induced by Rm is shown. Note the high number of lysosomes (ly) in the subtegument (in C large electron-dense areas in the soma region). (E and F) High-magnification images indicated by the boxed area in C. The presence of an isolation membrane (im) (E, unclosed cleft-like structure) and an autophagosome (a) (F) next to endoplasmic reticulum (er) cistern were observed. Arrows in (E) show the region of the isolation membrane where the two layers are attached together. mt, microtriches; glc, glycogen deposits; g, glycocalyx; dc, distal cytoplasm; mf, muscular fibres. Bars indicate 1 μm.

The finding that key autophagic genes are over-expressed in Rm-treated parasites led us to investigate possible mechanisms for their transcriptional regulation. The transcription factor FoxO participates in the promotion of autophagic activity, increasing the basal expression of several *atg* genes. A single FoxO transcription factor was identified in *E. granulosus* (Eg-FoxO, Fig. 4D and Supplementary Fig. S1), as described in other invertebrates such as *C. elegans* (known as DAF-16 -abnormal dauer formation protein 16), and *D. melanogaster* (named dFoxO). Along these same lines, Eg-*fox*O was over-expressed in Rm-treated parasites (Fig. 4B and D). Alignment of the amino acid sequence of Eg-FoxO with orthologous factors reveals that the DNA binding domain (Forkhead domain) and several phosphorylatable serine/threonine residues are highly conserved (Supplementary Fig. S1A and B). Therefore, all FoxOs share similar DNA binding specificity, with the core binding motif being defined as TTGTTTAC (Furuyama et al., 2000). We thus analysed Eg-FoxO transcriptional target candidates predicted by the 1 kb upstream survey of each *atg* gene in *Echinococcus* genomes. BLASTn analysis of the upstream sequences in Eg-*atg*8 and Eg-*atg*12 putative promoters (at 866 and 1031 bp with respect to the translational start codon, respectively) showed the conserved binding motif described for FoxO-activated genes (Supplementary Fig. S1C).

3.4. Molecular characterisation of predicted Eg-Atg proteins

Echinococcus autophagy-related proteins showed that all domains corresponding to specific functions were conserved, including the key amino acids involved in protein–protein or protein-membrane interactions (Supplementary Figs. S2–S10).

3.5. Expression pattern of Eg-Atg8 during the larval stage and in the microcyst development

Using a rabbit polyclonal antibody directed against the N-terminus of human MAP LC3β, the Eg-Atg8 proteins may be detected by immunoassays. A single band of the expected size at 14 kDa was identified, corresponding to Eg-Atg8.1 in both control and Rm-treated protoscoleces (Fig. 5A). Only in Rm-treated protoscoleces was a second more intense band with higher mobility detected. This band, named Eg-Atg8-PE, should correspond to Eg-Atg8.1 conjugated to PE, thus Atg8 is anchored to membranes. The bands

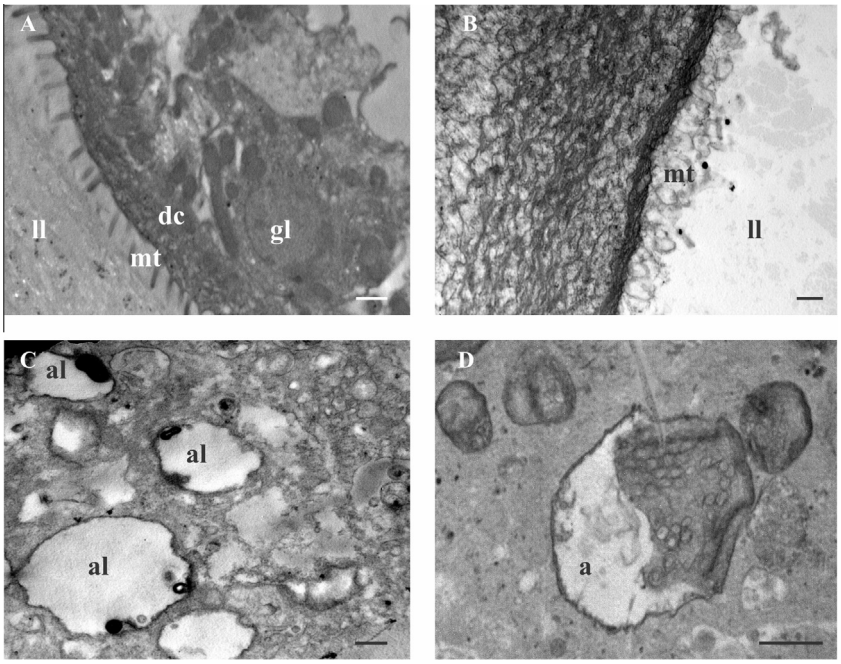

Fig. 3. Ultrastructure of rapamycin (Rm)-treated *Echinococcus granulosus* metacestodes. Transmission electron microscopy of control (A) and 20 μM Rm-treated metacestodes (B–D) are shown. Note the presence of autolysosomes (al) with lamellar stacks (in C) and an autophagosome (a) with a tubular array of lamellar structures in the germinal layer (in D). ll, laminal layer; gl, germinal layer; dc, distal cytoplasm; mt, microtriches. Bars indicate 0.5 μm.

were not observed when the strips were incubated with the secondary antibody alone (data not shown).

Immunohistochemical labelling showed that anti-Atg8 reactivity was localised in all tissues with a strong tegumental signal in both control (Fig. 5Bb) and Rm-treated protoscoleces (Fig. 5Bc). No signal was detected in the control sections that were only incubated with secondary antibody under the same conditions (Fig. 5Ba). In toto immunolocalisation assays allowed detection of Eg-Atg8.1 expression with both a diffuse and punctate staining (Fig. 5Bd–i). The expression was diffuse mainly in the cytoplasm of internal cellular territory of control protoscoleces. Fluorescent punctate images were often detected in tegument from control (Fig. 5Be) and Rm-treated protoscoleces (Fig. 5Bg–i). We observed an increase in the number of punctate structures in the tegument and flame cells of Rm-treated protoscoleces (Fig. 5Bg–i), in comparison with the control. At the beginning of vesicular differentiation, the number of puncta in the tegument decreased and the signal became mainly restricted to the bladder and flame cells (Fig. 5Bf). Non-specific fluorescent signal was detected in the rostellar hooks (Fig. 5Bf–i). The fluorescence pattern was not observed when the parasites were incubated with secondary antibody alone (Fig. 5Bd).

3.6. Analysis of Eg-Atg8.1 expression in calcareous corpuscles

Arsenic trioxide (As_2O_3), a prototype lysosome inducer and autophagic stressor (Bolt et al., 2010; Goussetis et al., 2010), was used to study the function and cellular activity of calcareous corpuscles in *E. granulosus* protoscoleces. In agreement with the morphological evidence of the corpuscle formation process, our SEM studies from sectioned protoscoleces showed cells at an initial developmental stage (a rod-shaped parenchyma cell with a central vacuole, Fig. 6A and B) and during a final lamellar step (a mature corpuscle with concentrically paired membranes bounded only by a thin layer of cytoplasm, Fig. 6A, C and D). EDX microanalysis demonstrated the co-localisation of arsenic with the main ionic components of the corpuscles: calcium, magnesium and phosphorus (Fig. 6E–H, and data not shown). A negative control without As_2O_3 was assayed (data not shown). Additionally, arsenic exposure increased key autophagic gene and Eg-*fox*O expression (Fig. 7A and B). qPCR showed higher mRNA expression levels for Eg-*atg*5 (twofold), Eg-*atg*6 (twofold), Eg-*atg*8.1 (fourfold), Eg-*atg*12 (fourfold), Eg-*atg*16 (twofold), and Eg-foxO (threefold) in 0.50 μM arsenic-treated protoscoleces than in controls (Fig. 7B). Finally, in accordance with the autophagic development stages, Eg-Atg8.1 expression was immunodetected in the central or peripheral cytoplasm of the calcareous corpuscles from Rm and arsenic-treated protoscoleces (Fig. 5Bg; Fig. 7C).

4. Discussion

Autophagy plays a role in cell survival and can be up-regulated in response to both external and intracellular factors. In fact, it intervenes actively in the larval development and arthropod and nematode embryogenesis (Meléndez and Levine, 2009; Malagoli et al., 2010). In this work, we studied the autophagy process that occurs in the larval stages of *E. granulosus*, at cellular and molecular levels, with the aim to analyse autophagy in cells that die under pharmacological treatment and special physiological conditions.

Paradoxically, autophagy can serve to protect cells but may also contribute to cell damage. Regarding the role of autophagy-associated cell death, the anti-echinococcal activity of Rm in metacestodes (Fig. 1A–C) is in agreement with the results obtained in protoscoleces (Cumino et al., 2010). Additionally, the gene expression of *Echinococcus* homologs of TOR and raptor was confirmed in protoscoleces and metacestodes (Fig. 1D). Since Rm was used to induce autophagy in *Echinococcus* larvae, and it is the major criterion used to identify TORC1-controlled events, our data are compatible with a conserved TORC1 in *Echinococcus*. This drug has been widely used to induce autophagy even under nutrient-rich conditions. In this regard, all in vitro experiments of this work were carried out with fresh culture medium, thereby suppressing basal

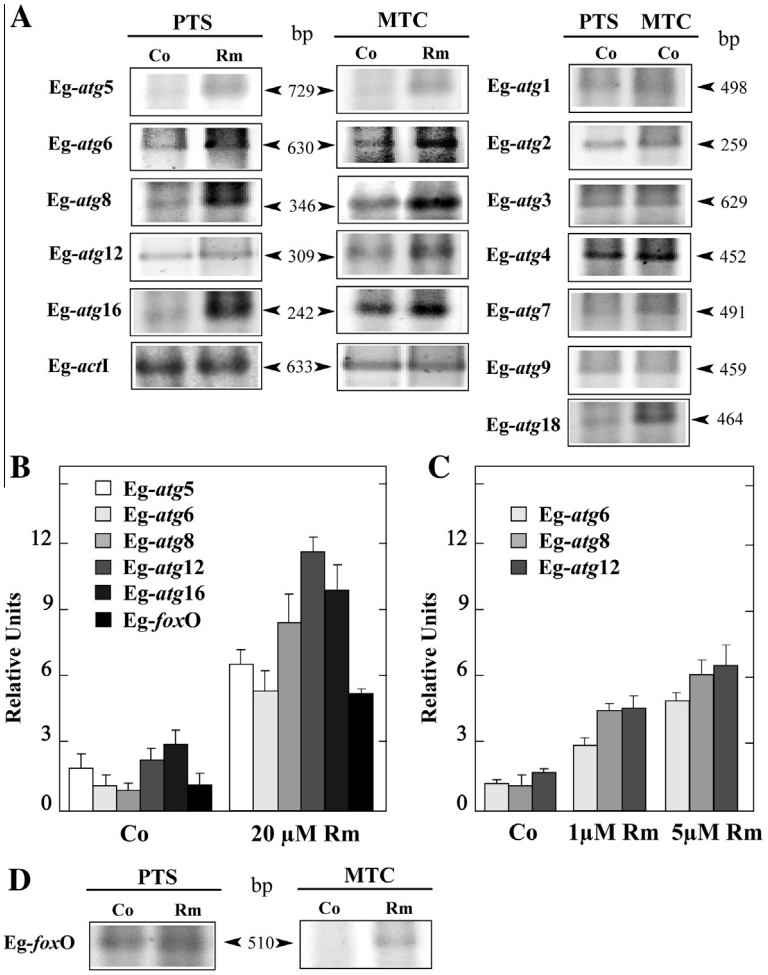

Fig. 4. Constitutive and rapamycin (Rm)-induced expression of autophagic genes in *Echinococcus granulosus* larval stages. (A) Reverse transcription–PCR analysis of *Eg-atg* genes from total RNA of protoscoleces (PTS) and metacestodes (MTC) incubated for 48 h under control conditions (Co) or treated with 20 μM Rm. Amplification of Eg-*actin I* (*act*I) was used as a loading control. Molecular sizes of amplicons are indicated with arrowheads. (B) Quantitative PCR was carried out under the same conditions as indicated in A. Values are means ± S.D. of three independent experiments. (C) Quantitative PCR analysis of *Eg-atg* genes from total RNA of protoscoleces incubated for 4 or 6 days under control conditions (Co) or treated with 5 μM or 1 μM Rm, respectively. (D) Reverse transcription–PCR assay of *E. granulosus* Forkhead box transcription factor class O (Eg-*fox*O), demonstrating its over-expression in Rm-treated parasites.

autophagy in *Echinococcus* larval stages. Further experiments with hydatid fluid and different starvation conditions should be carried out to study basal autophagy in this cestode.

Our results from in vitro pharmacological experiments using Rm in the micromolar range are consistent with autophagy induction and subsequent cell death by complete G1 arrest suppressing the phosphorylation of key TORC1 substrates in different cell types (Klein and Jackson, 2011; Voronin et al., 2012; Saqcena et al., 2013). Although the Rm primarily inhibits TORC1, chronic administration of the drug can inhibit TORC2 signaling by disrupting the association of TOR with the rapamycin-insensitive companion of TOR (rictor). This impairs the glucose homeostasis via insulin signal and contributes to the proapoptotic effects of the drug (Sarbassov et al., 2006; Lamming et al., 2012). In the recently released whole genome sequence of *Echinococcus* spp. (Tsai et al., 2013) a homolog of the rictor gene was identified (scaffold_003 and gene ID EgrG_000670800 in *E. granulosus*). This data suggests that TORC2 could also be assembled in the cestode. In the future, it will be important to determine the sensitivity level of Akt/PKB phosphorylation and the apoptosis induction during long treatments with Rm in *Echinococcus* larval stages, to estimate the TORC2 contribution to the death mechanism of this drug.

Autophagosome detection is the morphological hallmark of autophagy (Eskelinen et al., 2011). We performed TEM analysis to examine autophagic structures in Rm-treated parasites (Figs. 2 and 3). The earliest detectable autophagic element was the isolation membrane with open edges (an unclosed cleft-like structure, also called the "omegasome", Fig. 2E). Autophagosomes (elongation products of the isolation membrane, Figs. 2F and 3D) and autolysosomes (Fig. 3C) were also detected. As the endoplasmic reticulum is frequently observed in close proximity to autophagosomes, it has been proposed as the source of the autophagosome or the platform for autophagosome formation (Fig. 2E shows endoplasmic cisterns around autophagic structures) (Tooze and Yoshimori, 2010). In *C. elegans*, unclosed isolation membranes are very rarely observed, because the autophagic process is highly dynamic where the multi-step flux is constant. On the other hand, several reports of anti-echinococcal drug screening have demonstrated the increase in the number of autophagosomes, suggesting it is a general response to pharmacological stress (Rogan and Richards, 1986; Casado et al., 1996; Pérez-Serrano et al., 1997). Our experiments showed an Eg-Atg8 level increment proportional to the drug concentration, related to autophagy induction (Figs. 4B, C and 7A, B; Klionsky et al., 2012). As stated above, these observations could

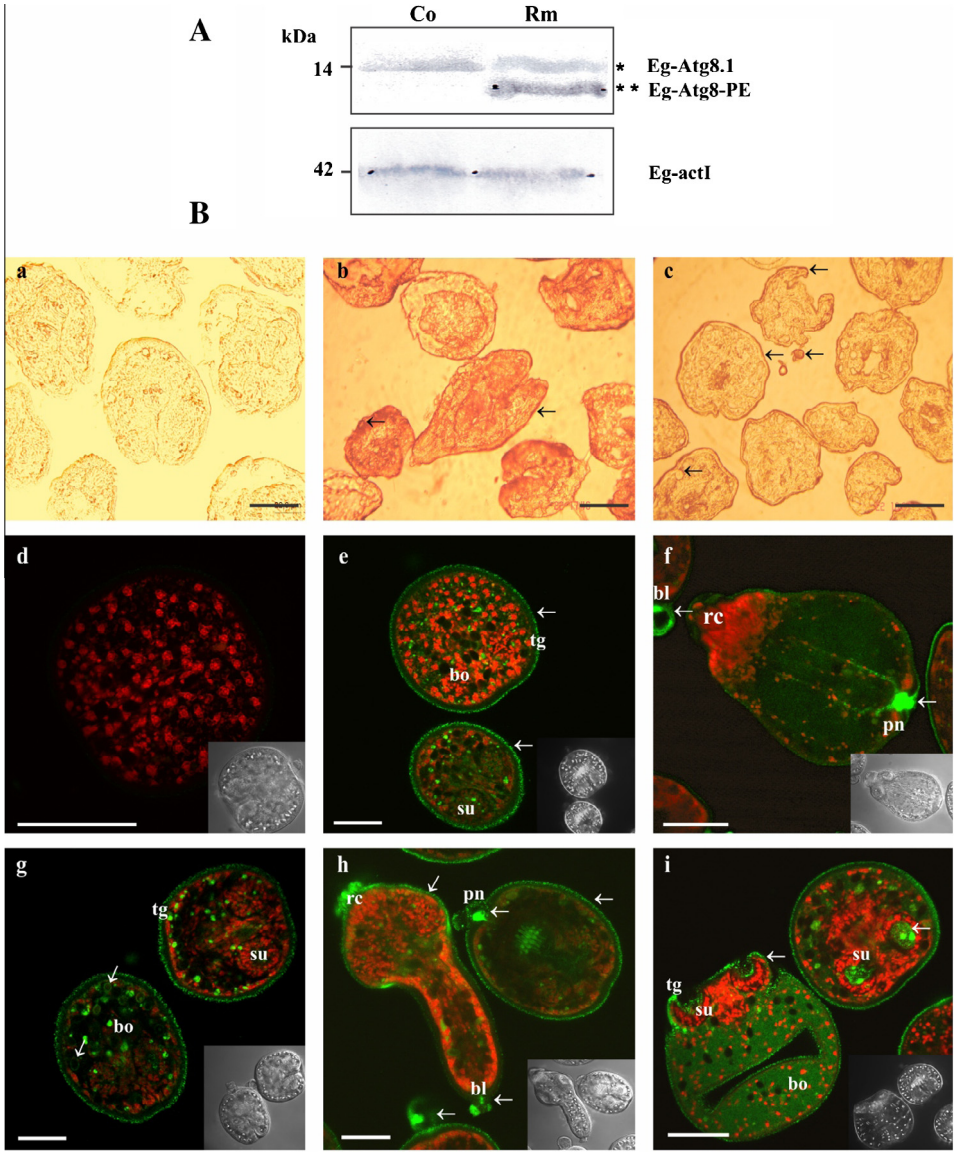

Fig. 5. Detection and in situ localisation of Eg-Atg8.1 from *Echinococcus granulosus* protoscoleces. (A) Immunoblot of Eg-Atg8.1 revealed with a heterologous antibody against human LC3. Total protein extracts from control (Co) and 20 μM rapamycin-treated protoscoleces (Rm) were loaded at 100 μg of total protein/lane. Both Eg-Atg8.1 and phosphatidylethanolamine-conjugated Eg-Atg8.1 (Eg-Atg8-PE) were detected. Polypeptide sizes are shown. (B) In situ localisation of Eg-Atg8.1 detected by immunohistochemistry with a secondary antibody conjugated with alkaline phosphatase (a–c) from histological sections (a, negative control; b, Co and c, Rm-treated parasites). Confocal images (d–i) correspond to in toto protoscolex assays revealed with an antibody conjugated with Alexa 488 – green fluorescence – and counterstained with propidium iodide – red fluorescence. Inset images correspond to transmission microscopy. (e) Protoscolex control, (g–i) Rm-treated protoscoleces, (f) pre-microcyst, (d) negative control. rc, rostellar cone; su, suckers; bo, body; tg, tegument; pn, protonephridial excretory system; bl, terminal bladder. Bars indicate 50 μm. Arrowheads in b and c and e–i indicate high expression regions of Eg-Atg8 in protoscoleces and pre-microcyst. (For interpretation of the references to colour in this figure legend, the reader is referred to the web version of this article.)

denote accumulation of autophagic structures due to inefficient completion of the catabolic process more than induction of autophagy (Klionsky et al., 2012). Similarly, as autophagy also contributes to lipid catabolism, the occurrence of lipid droplets as ultrastructural changes in these reports could be interpreted as an interruption of the autophagic flux (Singh and Cuervo, 2011).

A high degree of sequence conservation was observed between predicted *Echinococcus* autophagy-related proteins and eukaryotic orthologs (Supplementary Figs. S2–S10). By means of a hierarchical analysis using mammalian Atg proteins, (Jung et al., 2009) it has been demonstrated that the Atg1/Ulk1–2 complex (Ulk1–2, mAtg13, FIP200 and Atg101 proteins) functions at the most upstream step, and that it is phosphorylated and inactivated by TORC1. In starved animal cells or when TORC1 is specifically inhibited, these sites are dephosphorylated and Atg1/Ulk1–2 kinase activity increases, thus leading to Atg13 phosphorylation and autophagy initiation. In contrast to what is observed in yeast, in mammalian and insect cells direct interaction between raptor and Atg1/Ulk1–2 can be detected under nutrient-rich conditions (Jung et al., 2009; Alers et al., 2012). Only the Eg-Ulk2 complex component was identified in the *Echinococcus* genome (Fig. 4, Supplementary Tables S2 and Supplementary Fig. S3). Our ortholog prediction conditions (*E*-value cutoff $\leqslant 1e^{-25}$) did not allow us to identify FIP200, Atg101 and Atg13 encoding genes from the *Echinococcus* genome (Supplementary Table S2) in accordance with recent publications (Tsai et al., 2013). Besides the low sequence conservation, these proteins lack structural homology between human and *C. elegans* orthologs. Thus, functional studies of autophagy molecular mechanisms should be carried out in cestodes.

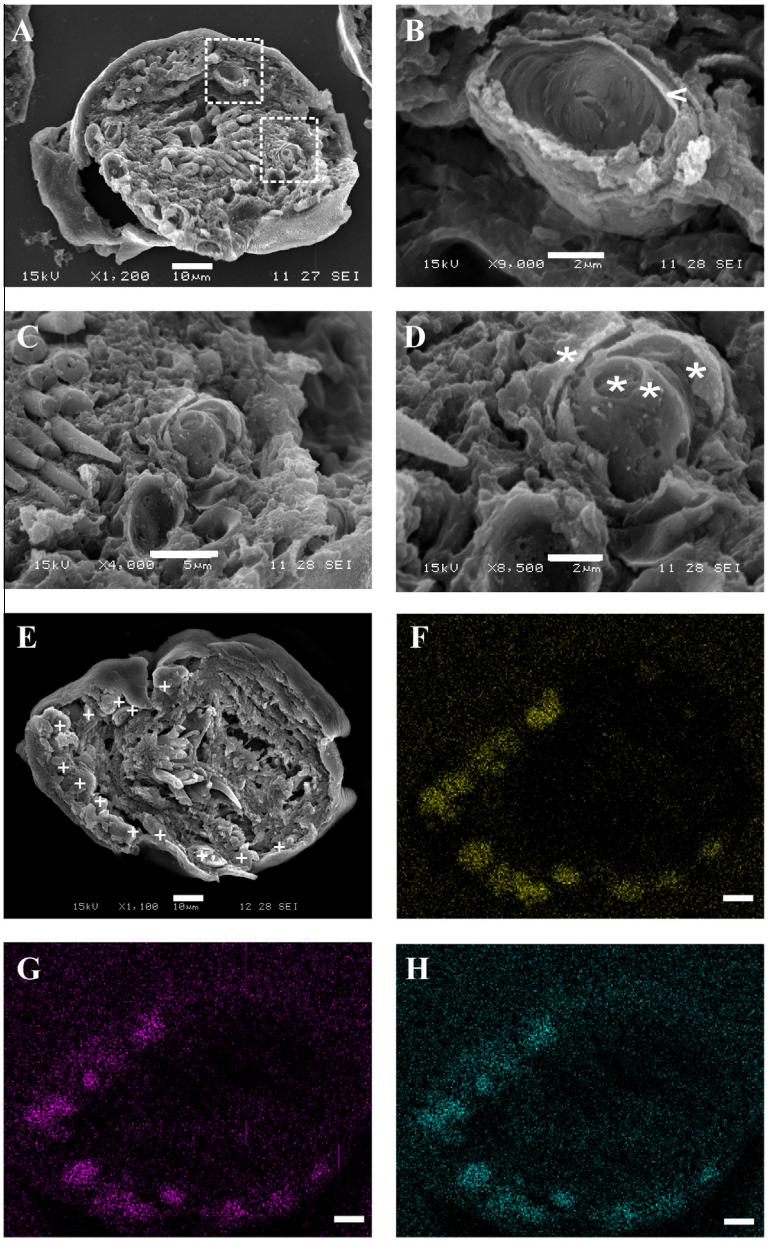

Fig. 6. Ultrastructure and microanalyses of the calcareous corpuscles from arsenic trioxide-treated protoscoleces of *Echinococcus granulosus*. (A–E) Scanning electron micrographs of a sectioned protoscolex (A and E) and its corpuscles (B–D). Boxed area in (A) is shown in high magnification images in (B) (cells in an initial development stage with large central vacuole, arrowhead) and in (C and D) (madure corpuscle with concentric membranes, indicated with asterisks). (F–H) Energy-dispersive X-ray elemental analysis of the calcareous corpuscles (indicated with "+") identified in sectioned protoscolex showed in (E). The predominant elements are calcium (F), magnesium (G), phosphorus (data not shown) and arsenic (H). Energy-dispersive X-ray spectrums of the images are in agreement with the reports by Smith and Richards (1993). Mg, 1.25 keV; As, 1.35 keV; P, 2.02 keV and Ca, 3.70 keV. Bars indicate 10 µm in A, E–H, 5 µm in C and 2 µm in B and D.

PI3P is essential for canonical autophagosome formation. In consequence, class III PI3K (Vps34 and Vps15) and PI3Ps are involved in autophagy (Taguchi Atarashi et al., 2010). Regarding the *Echinococcus* PI3K complex, only Eg-*atg*6 gene expression was analysed, and both Vps were in silico identified (Fig. 4 and Supplementary Table S2). Further studies are necessary to confirm the composition of the PI3K complex in *Echinococcus* sp. Other PI3P effectors in the autophagy pathway are the Atg18 family proteins. These proteins have typical WD-repeats and could interact with phosphoinositides through "FRRG" motifs. Conserved Eg-Atg18 and Eg-Atg2 proteins with possible membrane interaction sites could regulate the membrane traffic in a way similar to that observed in eukaryotic cells (Singh and Cuervo, 2011).

Two ubiquitin-like conjugation systems function at a late step of autophagosome formation, expansion and closure of the membrane. The conjugates Atg12-Atg5 and Atg8-lipidated serve as good markers to detect membrane structures during autophagy (Klionsky et al., 2012). The Atg8/LC3 reporter is used as a tool to detect autophagy in yeast and mammalian cells. In this work, western blotting was used to monitor changes in the non-lipidated (referred as the 'I' form) and lipidated (named the 'II' form or 'Atg8-PE') forms of Eg-Atg8 during Rm autophagy induction (Fig. 5A). Conjugated Atg8/LC3 is the only protein marker that is reliably associated with complete autophagosomes (Klionsky et al., 2012). In most organisms, Atg8 as well as LC3, GABARAP and GATE-16 are ubiquitin-like proteins initially synthesised with a C-terminal extension that is removed by the cysteine protease Atg4 exposing a glycine residue. According to genome data, Eg-Atg8.1 sequence shows an exposed C-terminal glycine residue similarly to the *C. elegans* LGG2 ortholog (Alberti et al., 2010). In nematodes, this fact did

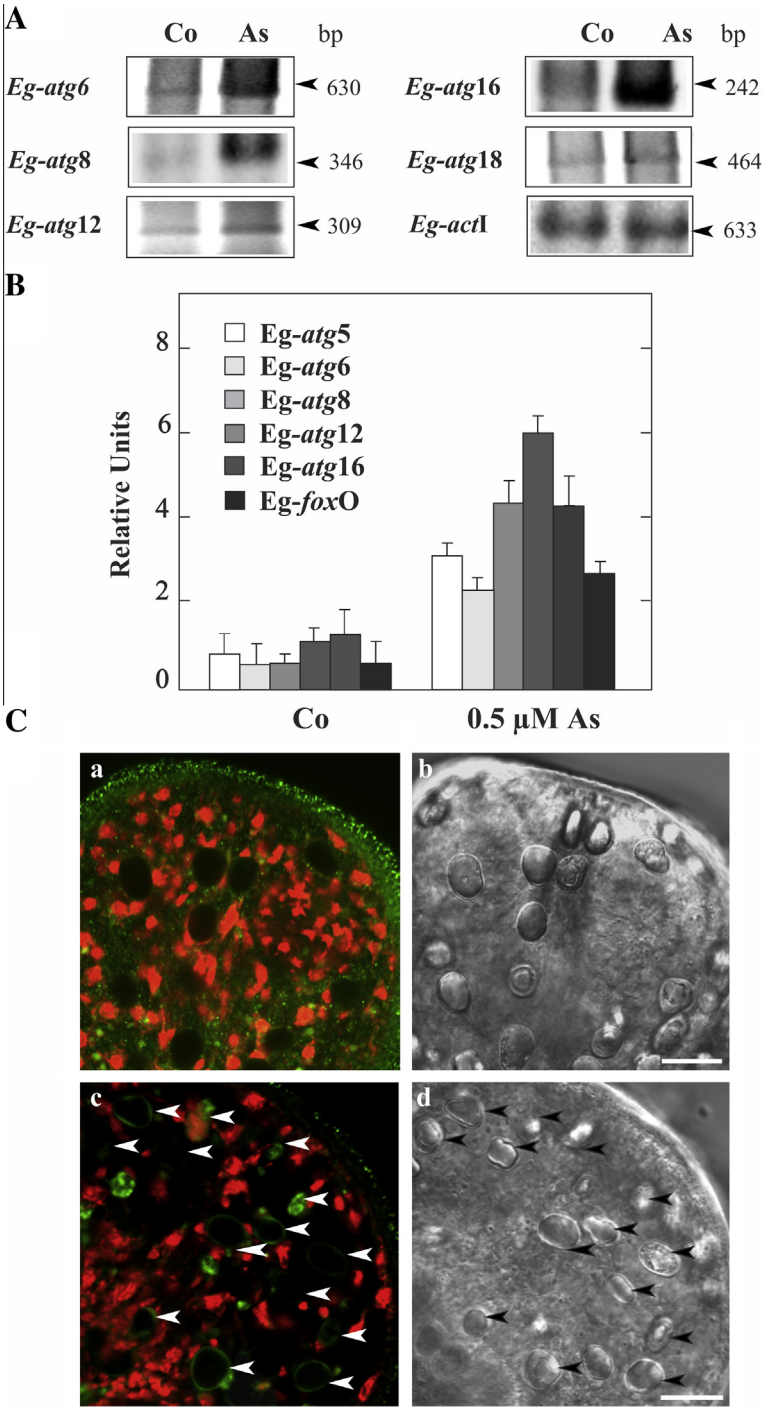

Fig. 7. Induced expression of key autophagic genes with arsenic trioxide in *Echinococcus granulosus* protoscoleces. (A) Reverse transcription–PCR analysis from total RNA of control (Co) and 3 µM arsenic trioxide (As) treated protoscoleces. Amplification of Eg-*act*I was used as a loading control. Molecular sizes of amplicons are indicated with arrowheads. (B) Quantitative PCR analysis of *Eg-atg* genes from total RNA of protoscoleces incubated for 12 h under control conditions (Co) or treated with 0.5 µM arsenic trioxide (As). (C) In situ localisation of Eg-Atg8.1 by confocal microscopy from control (a and b) and arsenic trioxide-treated protoscoleces (c andnb d). Confocal (a and c) and transmission (b and d) images correspond to in toto assays immunorevealed with a human anti-LC3 antibody conjugated with Alexa 488 – green fluorescence – and counterstained with propidium iodide – red fluorescence. Arrowheads indicate the Eg-Atg8.1 over-expression into calcareous corpuscles from treated protoscoleces. Bars indicate 10 µm. (For interpretation of the references to colour in this figure legend, the reader is referred to the web version of this article.)

not interfere with membrane conjugation or with the deconjugation function of Atg4 on Atg8 to regulate the level of free Atg8. Additionally, in toto immunodetection of Eg-Atg8 in cytoplasmic granules was also monitored in protoscoleces (Fig. 5B). A high expression level and punctate pattern were detected in the syncytial tegument and in several parenchymal cells of the soma in control and Rm-treated parasites (Fig. 5B, e–i). Another important observation was the presence of Eg-Atg8 punctate dot formations in the excretory system from Rm-treated parasites and vesicularised protoscoleces, which suggests that autophagy has a particular role in development towards vesicular differentiation. Particularly, the presence of Eg-Atg8 punctate images in control and vesicularised protoscoleces and the high gene expression level of *atg* genes from control samples (Fig. 4) suggest the occurrence of basal

autophagy in the larval stages and during parasite development. This catabolic process could be necessary during the *Echinococcus* larval stage and adult parasite development due to different reasons: a permanent nutritional dependence on the mammalian hosts, low cellular energy generation, hypoxia and oxidative stress as a common denominator (Virginio et al., 2012).

All homologs involved in the two ubiquitin-like pathways, except for Atg10, have been found in *E. granulosus*. Atg10 has neither been identified in *D. melanogaster* nor in *Apis mellifera* (Klionsky et al., 2012). A possible explanation is that the function of Atg10 could be compensated by Atg3 (Zhang et al., 2009). However, in the *Echinococcus* genome publication, Tsai et al. (2013) were able to annotate a homolog to *Echinococcus* Atg10. Eg-Atg3 might be able to recognise both Eg-Atg8 and Eg-Atg12, which share an ubiquitin-like fold and a highly conserved glycine residue at the C-terminal region (Supplementary Fig. S5).

The pharmacological induction of autophagy in *Echinococcus* cells is accompanied by an increase in the mRNA levels of autophagic genes, such as Eg-*atg*8 and Eg-*atg*12, as described in mammalian cells (Figs. 4A–C and 7A, B; Kouroku et al., 2007; Goussetis et al., 2010). In addition, these genes show conserved consensus sequences for FoxO binding in the region upstream of their translational start codon (Supplementary Fig. S1C). Thus, these autophagic genes are potential Eg-FoxO target genes. Interestingly, Eg-FoxO over-expression could promote autophagy by up-regulating specific gene expression programs in agreement with other cellular systems (Figs. 4B, C, 7B and Supplementary Fig. S1) (Mammucari et al., 2007). Mammalian FoxO factors (FoxO1, FoxO3a, FoxO4 and FoxO6) are homologs of the *C. elegans* DAF-16 and of *Drosophila* dFoxO. Specifically, FoxO1 and FoxO3 induce the transcription of multiple autophagic genes, including *LC3B*, *Gabarapl1*, *atg12*, *atg4B*, *vps34*, *ulk2*, *beclin 1*, and *Bnip3l*, directly binding to their promoters to activate gene transcription. In addition, Rm and arsenic trioxide induced over-expression of Eg-*atg*5, Eg-*atg*6, Eg-*atg*16 and Eg-*atg*18 (Figs. 4A–C, 7A, B and data not shown), but caused no changes in the transcriptional expression level of Eg-*atg*1 to Eg-*atg*4 and Eg-*atg*9 in both larval stages (Fig. 4A and data not shown). These results are concordant with transcriptional up-regulation of *atg*5, *atg*6 and *atg*8 in *D. melanogaster* and *B. mori* larval development (Denton et al., 2010). Interestingly, in mammalian cells, the expression of *atg*8, *atg*9 and *atg*18 and other genes involved in lysosomal biogenesis appeared to be direct targets by the basic helix–loop–helix transcription factor EB (TFEB) because they carry at least one TFEB target site in their promoters (Settembre et al., 2011). TFEB acts as a master gene of lysosomal and autophagic genes and is regulated by starvation. Expression and activity of TFEB orthologs from *Echinococcus* sp. should be analysed in subsequent experiments. In agreement with the metazoan cell system, in *Echinococcus* cells, autophagy could be regulated by non-transcriptional inhibition through TOR and transcription-dependent up-regulation via FoxOs and/or TFEB proteins (He and Klionsky, 2009).

Finally, it has been proposed that the biomineral concretions termed calcareous corpuscles present in cestode tissues could be formed, beginning with the autophagic breakdown of the cytoplasm (McCullough and Fairweather, 1987). In this line of evidence, our SEM images showed the presence of two formation stages of calcareous corpuscles in sectioned protoscoleces: one with a full-size central vacuole and the other with concentric lamellae in the parenchyma cell (Fig. 6A–D). These results are in agreement with TEM data of calcareous corpuscles from several cestode species including *E. granulosus* (von Brand et al., 1960; Timofeev, 1964; McCullough and Fairweather, 1987; Smith and Richards, 1993). When autophagy is activated after endoplasmic reticulum stress, formation of multilamellar structures within the autophagosomes can be observed (Ogata et al., 2006). These findings differ from those in cells deprived of amino acids (Ogata et al., 2006). This situation could be coincidental with the formation process of calcareous corpuscles. In our experiment the low expression of Eg-Atg8 in untreated calcareous corpuscles and/or the incomplete permeabilisation process of these biomineralised cells, did not allow to immunodetect this protein in the control sample (Figs. 5Be and 7C). As arsenic trioxide exposure in myeloid leukaemia and glioma cells promotes autophagy development (Bolt et al., 2010; Goussetis et al., 2010), we used this drug to increase this catabolic process in calcareous corpuscles and test the autophagic hypothesis. In Rm and arsenic-treated protoscoleces, we detected an increase in the autophagic gene expression and a high Eg-Atg8 polypeptide level in the free cytoplasmic matrix of corpuscles (Figs. 5Bg and 7B). These results allow us to verify the autophagic activity of these specialised cells, leading to reconsideration of the theory proposed by McCullough and Fairweather (1987) on corpuscle autophagic development. Calcareous corpuscles are assumed to have different roles in the physiology of tapeworms. They might serve either the focal deposition of excessive amounts of calcium, protecting larvae against calcification, as reservoirs of carbonate and phosphate, or as excretory dumps. Our experiments with arsenic trioxide also demonstrated that calcareous corpuscles are ion accumulation sites, suggesting a possible role in heavy metal bioaccumulation and detoxification, similar to that described for other biomineralised cells or granules rich in calcium, phosphate and magnesium (Kegley et al., 1970; Sures et al., 1997).

Understanding the functional context of autophagy is important for parasitic helminths, since it can either be a constitutive homeostatic process, a stress-induced cellular survival mechanism, or a stress-induced mechanism tied to cell death, depending on the particular context in which the process occurs. Autophagy must play an important role in these parasites, where the starvation conditions and other forms of stress could induce the metabolic reprogramming throughout their life cycle when they have to adapt to the different nutritional environments in different hosts. There is considerable interest in this pathway as a target for therapeutic intervention for a variety of human pathologies. Although there is high amino acid sequence conservation in *Echinococcus* autophagy-related proteins, future studies should lead to differential structure determination of parasite ATG proteins, the in silico design and the synthesis of selective inhibitors to promote drug discovery aimed against neglected parasitic diseases.

Acknowledgements

The authors gratefully acknowledge the excellent knowledge transfer in animal care by Dr. Goya A. (SENASA, Argentina), the technical assistance in the use of electron microscopes by the Centro Regional de Investigaciones Básicas y Aplicadas de Bahía Blanca (CRIBABB) and MSc. Ing. J. F. Vilá. We are also grateful for the use of facilities at the IIB-Conicet-UNMdP and at the INBIOTEC-CONICET-FIBA, Argentina. This work was supported by CONICET (Grant PIP No. 0029), Universidad Nacional de Mar del Plata (Grant EXA 572/12) and ANPCyT (PICT 2012, No. 2668) Argentina. The *E. multilocularis* and *E. granulosus* genome sequence data mentioned was produced by the Pathogen Sequencing Group of the Wellcome Trust Sanger Institute (Program of Helminth Sequencing; project manager: Dr. Matt Berriman).

Appendix A. Supplementary data

Supplementary data associated with this article can be found, in the online version, at http://dx.doi.org/10.1016/j.ijpara.2014.02.007.

References

Al-Adhami, B.H., Noble, C., Sharaf, O., Thornhill, J., Doenhoff, M.J., Kusel, J.R., 2005. The role of acidic organelles in the development of schistosomula of *Schistosoma mansoni* and their response to signalling molecules. Parasitology 130, 309–322.

Alberti, A., Michelet, X., Djeddi, A., Legouis, R., 2010. The autophagosomal protein LGG-2 acts synergistically with LGG-1 in dauer formation and longevity in *C. elegans*. Autophagy 6, 622–633.

Alers, S., Löffler, A.S., Wesselborg, S., Stork, B., 2012. Role of AMPK–mTOR–Ulk1/2 in the regulation of autophagy: cross talk, shortcuts, and feedbacks. Mol. Cell. Biol. 32, 2–11.

Betz, C., Hall, M.N., 2013. Where is mTOR and what is it doing there? J. Cell Biol. 25, 563–574.

Bolt, A.M., Byrd, R.M., Klimecki, W.T., 2010. Autophagy is the predominant process induced by arsenite in human lymphoblastoid cell lines. Toxicol. Appl. Pharm. 244, 366–373.

Casado, N., Pérez-Serrano, J., Denegri, G., Rodríguez-Caabeiro, F., 1996. Development of chemotherapeutic model for the *in vitro* screening of drugs against *Echinococcus granulosus* cysts: the effects of an albendazole–albendazole sulphoxide combination. Int. J. Parasitol. 26, 59–65.

Choi, J., Chen, J., Schreiber, S.L., Clardy, J., 1996. Structure of the FKBP12–rapamycin complex interacting with binding domain of human FRAP. Science 273, 239–242.

Cumino, A.C., Lamenza, P., Denegri, G.M., 2010. Identification of functional FKB protein in *Echinococcus granulosus*: its involvement in the protoscolicidal action of rapamycin derivates and in calcium homeostasis. Int. J. Parasitol. 40, 651–661.

Denton, D., Shravage, B.V., Simin, R., Baehrecke, E.H., Kumar, S., 2010. Larval midgut destruction in *Drosophila*: not dependent on caspases but suppressed by the loss of autophagy. Autophagy 6, 163–165.

Eskelinen, E.L., Reggiori, F., Baba, M., Kovács, A.L., Seglen, P.O., 2011. Seeing is believing: the impact of electron microscopy on autophagy research. Autophagy 7, 935–956.

Furuyama, T., Nakazawa, T., Nakano, I., Mori, N., 2000. Identification of the differential distribution patterns of mRNAs and consensus binding sequences for mouse DAF-16 homologues. Biochem. J. 349, 629–634.

Goussetis, D.J., Altman, J.K., Glaser, H., McNeer, J.L., Tallman, M.S., Platanias, L.C., 2010. Autophagy is a critical mechanism for the induction of the antileukemic effects of arsenic trioxide. J. Biol. Chem. 285, 29989–29997.

Hara, K., Maruki, Y., Long, X., Yoshino, K.I., Oshiro, N., Hidayat, S., Tokunaga, C., Avruch, J., Yonezawa, K., 2002. Raptor, a binding partner of target of rapamycin (TOR), mediates TOR action. Cell 110, 177–189.

He, C., Klionsky, D.J., 2009. Regulation mechanisms and signaling pathways of autophagy. Annu. Rev. Genet. 43, 67–93.

Jung, C.H., Jun, C.B., Ro, S.H., Kim, Y.M., Otto, N.M., Cao, J., Kundu, M., Kim, D.H., 2009. ULK–Atg13–FIP200 complexes mediate mTOR signaling to the autophagy machinery. Mol. Biol. Cell 20, 1992–2003.

Kegley, L.M., Baldwin, J., Brown, B.W., Berntzen, A.K., 1970. *Mesocestoides corti*: environmental cation concentration in calcareous corpuscles. Exp. Parasitol. 27, 88–94.

Klein, K.A., Jackson, W.T., 2011. Human rhinovirus 2 induces the autophagic pathway and replicates more efficiently in autophagic cells. J. Virol. 85, 9651–9654.

Klionsky, D.J., Abdalla, F.C., Abeliovich, H., Abraham, R.T., Acevedo-Arozena, A., Adeli, K., Agholme, L., Agnello, M., Agostinis, P., Aguirre-Ghiso, J.A., Ahn, H.J., Ait-Mohamed, O., Ait-Si-Ali, S., Akematsu, T., Akira, S., Al-Younes, H.M., Al-Zeer, M.A., Albert, M.L., Albin, R.L., Alegre-Abarrategui, J., Aleo, M.F., Alirezaei, M., Almasan, A., Almonte-Becerril, M., Amano, A., Amaravadi, R., Amarnath, S., Amer, A.O., Andrieu-Abadie, N., Anantharam, V., Ann, D.K., Anoopkumar-Dukie, S., Aoki, H., Apostolova, N., Arancia, G., Aris, J.P., Asanuma, K., Asare, N.Y., Ashida, H., Askanas, V., Askew, D.S., Auberger, P., Baba, M., Backues, S.K., Baehrecke, E.H., Bahr, B.A., Bai, X.Y., Bailly, Y., Baiocchi, R., Baldini, G., Balduini, W., Ballabio, A., Bamber, B.A., et al., 2012. Guidelines for the use and interpretation of assays for monitoring autophagy. Autophagy 8, 445–544.

Kouroku, Y., Fujita, E., Tanida, I., Ueno, T., Isoai, A., Kumagai, H., Ogawa, S., Kaufman, R.J., Kominami, E., Momoi, T., 2007. ER stress (PERK/eIF2α phosphorylation) mediates the polyglutamine-induced LC3 conversion, an essential step for autophagy formation. Cell Death Differ. 14, 230–239.

Kovacs, A.L., Zhang, H., 2010. Role of autophagy in *Caenorhabditis elegans*. FEBS Lett. 584, 1335–1341.

Lamming, D.W., Ye, L., Katajisto, P., Goncalves, M.D., Saitoh, M., Stevens, D.M., Davis, J.G., Salmon, A.B., Richardson, A., Ahima, R.S., Guertin, D.A., Sabatini, D.M., Baur, J.A., 2012. Rapamycin-induced insulin resistance is mediated by mTORC2 loss and uncoupled from longevity. Science 335, 1638–1643.

Malagoli, D., Abdalla, F.C., Cao, Y., Feng, Q., Fujisaki, K., Gregorc, A., Matsuo, T., Nezis, I.P., Papassideri, I.S., Sass, M., Silva-Zacarin, E.C., Tettamant, G., Umemiya-Shirafuji, R., 2010. Autophagy and its physiological relevance in arthropods: current knowledge and perspectives. Autophagy 6, 575–588.

Mammucari, C., Milan, G., Romanello, V., Masiero, E., Rudolf, R., Del Piccolo, P., Burden, S.J., Di Lisi, R., Sandri, C., Zhao, J., Goldberg, A.L., Schiaffino, S., Sandri, M., 2007. FoxO3 controls autophagy in skeletal muscle *in vivo*. Cell Metab. 6, 458–471.

McCullough, J.S., Fairweather, I., 1987. The structure, composition, formation and possible functions of calcareous corpuscles in *Trilocularia acanthiaevulgaris* Olsson 1867 (Cestoda, Tetraphyllidea). Parasitol. Res. 74, 175–182.

Meléndez, A., Levine, B., 2009. Autophagy in *C. elegans*. WormBook 24, 1–26.

Mizushima, N., Yoshimori, T., Ohsumi, Y., 2011. The role of Atg proteins in autophagosome formation. Annu. Rev. Cell Dev. Biol. 27, 107–132.

Nakatogawa, H., Ichimura, Y., Ohsumi, Y., 2007. Atg8, a ubiquitin-like protein required for autophagosome formation, mediates membrane tethering and hemifusion. Cell 130, 165–178.

Nicolao, M.C., Denegri, G.M., Cárcamo, J.G., Cumino, A.C., 2014. P-glycoprotein expression and pharmacological modulation in larval stages of *Echinococcus granulosus*. Parasitol. Int. 63, 1–8.

Nyfeler, B., Bergman, P., Triantafellow, E., Wilson, C.J., Zhu, Y., Radetich, B., Finan, P.M., Klionsky, D.J., Murphy, L.O., 2011. Relieving autophagy and 4EBP1 from rapamycin resistance. Mol. Cell. Biol. 31, 2867–2876.

Ogata, M., Hino, S., Saito, A., Morikawa, K., Kondo, S., Kanemoto, S., Murakami, T., Taniguchi, M., Tanii, I., Yoshinaga, K., Shiosaka, S., Hammarback, J.A., Urano, F., Imaizumi, K., 2006. Autophagy is activated for cell survival after endoplasmic reticulum stress. Mol. Cell. Biol. 26, 9220–9231.

Pérez-Serrano, J., Denegri, G., Casado, N., Rodriguez-Caabeiro, F., 1997. *In vivo* effect of oral albendazole and albendazole sulphoxide on development of secondary echinococcosis in mice. Int. J. Parasitol. 27, 1341–1345.

Richards, K.S., Arme, C., Bridges, J.F., 1984. *Echinococcus granulosus equinus*: variation in the germinal layer of murine hydatids and evidence of autophagy. Parasitology 89, 35–48.

Rogan, M.T., Richards, K.S., 1986. *Echinococcus granulosus*: *in vitro* effect of monensin on the tegument of the protoscolex. Parasitology 93, 347–355.

Saqcena, M., Menon, D., Patel, D., Mukhopadhyay, S., Chow, V., Foster, D.A., 2013. Amino acids and mTOR mediate distinct metabolic checkpoints in mammalian G1 cell cycle. PLoS One 8, e74157.

Sarbassov, D.D., Ali, S.M., Sengupta, S., Sheen, J.H., Hsu, P.P., Bagley, A.F., Markhard, A.L., Sabatini, D.M., 2006. Prolonged rapamycin treatment inhibits mTORC2 assembly and Akt/PKB. Mol. Cell 21, 159–168.

Settembre, C., Di Malta, C., Polito, V.A., Garcia Arencibia, M., Vetrini, F., Erdin, S., Erdin, S.U., Huynh, T., Medina, D., Colella, P., Sardiello, M., Rubinsztein, D.C., Ballabio, A., 2011. TFEB links autophagy to lysosomal biogenesis. Science 332, 1429–1433.

Singh, R., Cuervo, A.M., 2011. Autophagy in the cellular energetic balance. Cell Metab. 4, 495–504.

Smith, S.A., Richards, K.S., 1993. Ultrastructure and microanalyses of the calcareous corpuscles of the protoscoleces of *Echinococcus granulosus*. Parasitol. Res. 79, 245–250.

Sures, B., Taraschewski, H., Siddall, R., 1997. Heavy metal concentrations in adult acanthocephalans and cestodes compared to their fish hosts and to established free living bioindicators. Parassitologia 39, 213–218.

Taguchi Atarashi, N., Hamasaki, M., Matsunaga, K., Omori, H., Ktistakis, N.T., Yoshimori, T., Noda, T., 2010. Modulation of local PtdIns3P levels by the PI phosphatase MTMR3 regulates constitutive autophagy. Traffic 11, 468–478.

Timofeev, V., 1964. Electron-microscopic studies on plerocercoid calcareous corpuscles in sexually-mature *Schistocephalus pungitii*. Dokl. Akad. Nauk SSSR 11, 1244–1247.

Tooze, S.A., Yoshimori, T., 2010. The origin of the autophagosomal membrane. Nat. Cell Biol. 12, 831–835.

Tsai, I.J., Zarowiecki, M., Holroyd, N., Garciarrubio, A., Sanchez-Flores, A., Brooks, K.L., Tracey, A., Bobes, R.J., Fragoso, G., Sciutto, E., Aslett, M., Beasley, H., Bennett, H.M., Cai, J., Camicia, F., Clark, R., Cucher, M., De Silva, N., Day, T.A., Deplazes, P., Estrada, K., Fernández, C., Holland, P.W., Hou, J., Hu, S., Huckvale, T., Hung, S.S., Kamenetzky, L., Keane, J.A., Kiss, F., Koziol, U., Lambert, O., Liu, K., Luo, X., Luo, Y., Macchiaroli, N., Nichol, S., Paps, J., Parkinson, J., Pouchkina-Stantcheva, N., Riddiford, N., Rosenzvit, M., Salinas, G., Wasmuth, J.D., Zamanian, M., Zheng, Y.The *Taenia solium* Genome Consortium, Cai, X., Soberón, X., Olson, P.D., Laclette, J.P., Brehm, K., Berriman, M., 2013. The genomes of four tapeworm species reveal adaptations to parasitism. Nature 496, 57–63.

Virginio, V.G., Monteiro, K.M., Drumond, F., de Carvalho, M.O., Vargas, D.M., Zaha, A., Ferreira, H.B., 2012. Excretory/secretory products from *in vitro*-cultured *Echinococcus granulosus* protoscoleces. Mol. Biochem. Parasitol. 183, 15–22.

von Brand, T., Mercado, T.I., Nylen, M.U., Scott, D.B., 1960. Observations on function, composition, and structure of cestode calcareous corpuscles. Exp. Parasitol. 9, 205–214.

Voronin, D., Cook, D.A., Steven, A., Taylor, M.J., 2012. Autophagy regulates *Wolbachia* populations across diverse symbiotic associations. Proc. Natl. Acad. Sci. U.S.A. 19 (109), 1638–1646.

Xie, Z., Klionsky, D.J., 2007. Autophagosome formation: core machinery and adaptations. Nat. Cell Biol. 9, 1102–1109.

Yang, Z., Klionsky, D.J., 2010. Mammalian autophagy: core molecular machinery and signaling regulation. Curr. Opin. Cell Biol. 22, 124–131.

Zhang, X., Hu, Z.Y., Li, W.F., Li, Q.R., Deng, X.J., Yang, W.Y., Cao, Y., Zhou, C.Z., 2009. Systematic cloning and analysis of autophagy-related genes from the silkworm *Bombyx mori*. BMC Mol. Biol. 10, 50.